Version of Record: https://www.sciencedirect.com/science/article/pii/S0584854721000033
Manuscript_817a261749a8c351095b1e00788984ff

Field investigation of volcanic deposits on Vulcano, Italy using a handheld laser-induced breakdown spectroscopy instrument

Kristin Rammelkamp[a,b], Susanne Schröder[a,b], Gianluigi Ortenzi[c,d], Alessandro Pisello[e], Katrin Stephan[c], Mickael Baqué[c], Heinz-Wilhelm Hübers[a,f], Olivier Forni[b], Frank Sohl[c], Laurenz Thomsen[g], Vikram Unnithan[g]

[a] *Deutsches Zentrum für Luft- und Raumfahrt (DLR), Institut für Optische Sensorsysteme, Berlin, Germany*
[b] *Institut de Recherche en Astrophysique et Planétologie, Toulouse, France*
[c] *Deutsches Zentrum für Luft- und Raumfahrt (DLR), Institut für Planetenforschung, Berlin, Germany*
[d] *Freie Universität Berlin, Department of Earth Sciences, Berlin, Germany*
[e] *University of Perugia, Department of Physics and Geology, Perugia, Italy*
[f] *Humboldt-Universität zu Berlin, Department of Physics, Berlin, Germany*
[g] *Jacobs University Bremen, Department of Physics and Earth Sciences, Bremen, Germany*

Abstract

Laser-induced breakdown spectroscopy (LIBS) is an important analytical technique in a variety of fields ranging from in-situ terrestrial geological field investigations to robotic exploration missions of extraterrestrial bodies such as Mars. In this study, the performance of a commercial handheld LIBS instrument was evaluated during an international summer school in 2019 that focused on the exploration of extreme environments on Earth and in space. Several sites on the Eolian island Vulcano (Italy) were investigated with different spectroscopic methods including LIBS. We focus here on the exploration of one particular outcrop with LIBS, where layered and colored ash deposits were observed. Furthermore, a laboratory study was performed

© 2021 published by Elsevier. This manuscript is made available under the CC BY NC user license
https://creativecommons.org/licenses/by-nc/4.0/

to investigate and validate the effect of varying distance of the instrument to the sample. Unsupervised principal component analysis (PCA) for data exploration showed that elemental variations between the layers of the outcrop can be observed with the LIBS data from the handheld instrument. This was further confirmed by a layer-by-layer analysis of elemental correlations and depositional trends. Geologically relevant major elements such as Si, Al, Ca, Fe, K, Mg, and Na could be identified but also minor and trace elements such as F, Li, Mn, and Sr. Our results also show that the effects of varying distances of the instrument to the sample are critical for the quality of the data acquired and hence pose significant challenges to the analysis and interpretation. We propose a dedicated data pre-processing approach, which includes the masking of emission lines of Ar from the locally induced Ar atmosphere, as a possible solution to overcome this challenge. Overall, this study provides a better understanding of the performance and limitations of a handheld LIBS instrument, particularly in the context of future terrestrial and planetary field investigations.

Keywords: LIBS, portable, in-field, elemental analysis, geochemical, ash layers

1. Introduction

For fast multi-elemental analysis, laser-induced breakdown spectroscopy (LIBS) is a powerful technique in various fields and applications [1], for example, in the steel [2] and nuclear industry [3], in food analysis [4], and in cultural heritage [5]. Another important application of LIBS is the geochemical analysis of samples in laboratories or samples in their geological context

in the field [6–8]. Geomaterial analysis in the field extends even to applications beyond Earth and LIBS gains more and more relevance for applications during the robotic exploration of extraterrestrial bodies. The first LIBS instrument for space exploration is the ChemCam instrument [9, 10], which is part of the scientific payload of NASA's Mars Science Laboratory (MSL), also known as Curiosity, and which has been analyzing the Martian surface since its landing in 2012 in Gale crater [11].

The LIBS technique is sensitive to atmospheric conditions where in particular the thin atmosphere at Mars' surface (7 mbar of mainly CO_2) is close to ideal for LIBS analysis [12]. There will be an enhanced follow-up instrument to ChemCam called SuperCam on NASA's Mars 2020 mission [13] and other LIBS instruments are planned and proposed for the exploration of different extraterrestrial objects [14–18]. Planetary exploration using LIBS instruments is envisaged for in-situ geochemical analysis of superficial rocks and soils in order to reconstruct the geological history of a particular site on the extraterrestrial body, similar to geochemical investigations on Earth.

Compared with other analytical methods, the strength of the LIBS technique lies in its instrumental simplicity, apparent ease of use, and versatility. For LIBS, a pulsed high-power laser is focused onto the surface of the target resulting in the ablation of material which further evolves into a micro-plasma. Excited atoms, ions, and simple molecules in the plasma emit a characteristic radiation from which the elemental composition of the target can be derived by spectral analysis [19]. In general, the irradiance threshold for the breakdown depends on the material properties but for solid targets an irradiance of $\approx 1\,\mathrm{GW\,cm^2}$ is considered to produce stable LIBS

plasmas suited for analysis [20, 8]. Usually, only optical access is necessary for analyzing samples with LIBS and sample preparation is not mandatory, nevertheless, LIBS results can be substantially improved by using dedicated sample preparation strategies [21, 6, 22]. But still, the possibility to measure without the need for sample preparation makes LIBS especially useful for applications where samples are difficult to access, or where targets are to be analyzed in their original context or when a particularly quick analysis is required.

Besides its high ease of use, the LIBS technique has several advantages for geochemical in-situ investigations. For example, while light elements with atomic number < 6 are challenging to detect with other elemental analysis methods such as electron micro probe [23] or alpha particle x-ray spectrometry [24], LIBS is sensitive to all elements including H. Furthermore, all elements can be simultaneously detected in real time which enables fast on-site multi-elemental analysis. The sampling area of LIBS instruments depends on the laser spot size on the sample surface which is usually in the range of 50-300 μm. This allows to detect changes in the elemental composition and therefore mineral variations on a small scale, and to investigate even small sized grains and features. The capability of using LIBS in the field without the need to collect samples, is a great benefit of LIBS for geochemical analysis [8, 6].

Nevertheless, the LIBS technique has also some challenges. These arise mainly from the sensitivity of the LIBS plasma to chemical and physical properties of the sample, also known as matrix effects, as well as to experimental parameters and conditions [19, 20, 8]. In particular for the complex geologi-

cal samples, this results typically in a low reproducibility of LIBS data which can then affect the accuracy of calibration models used for predicting elemental abundances [25]. Besides analytical approaches for reducing the influence of matrix effects, statistical methods such as principal component analysis (PCA) and partial least squares regression (PLS-R) are standard methods in LIBS data analysis [26].

For this study, LIBS data was collected during an interdisciplinary summer school held on Vulcano (Eolian Islands, Italy) in June 2019. The summer school focused on the robotic exploration of extreme environments ranging from the deep sea to planetary analogues. Vulcano offers a broad range of volcanic terrains, morphology and rock types for such planetary analog studies [27]. The geological evolution of Vulcano commences from 127 ka to present days, with the last major eruptive phase occurring in 1890 [27]. A number of eruptive episodes developed the present day morphology of the island, consisting of two intersecting caldera in the southern and central part of the island, and a smaller, more recent cone complex to the North, called Vulcanello. On Vulcano, a broad chemical variability of igneous products can be found, ranging from basalt to rhyolite, and including particularly alkaline products such as shoshonite and trachyte [28]. Hence, Vulcano is an ideal site to test new instruments and methods for geochemical investigation as it is possible to analyze a broad range of volcanic deposits, both in chemistry and physical properties. Different sites on the island were not only investigated with LIBS but also with other spectroscopic instruments such as a visible and near infrared spectro-radiometer and a portable Raman spectrometer. The three spectroscopic methods are of high interest for planetary in-situ explo-

ration by mobile spacecrafts. A combined analysis of the data from all three spectroscopic techniques is planned and first results can be found in [29, 30]. Besides the spectroscopic analysis, further experiments were conducted with the general objective of the summer school to learn about robotic exploration for space and deep sea research. Regarding the robotic in-situ exploration of planets and other bodies in the Solar System, the island offers the possibility to study various planetary analogous sites with igneous minerals in volcanic ashes, glasses or just lava flows that might be found similarly on other bodies showing volcanism in the Solar System [31]. Evaluating the performance, applicability, and potential of the different spectroscopic methods at this place has therefore a high relevance and can provide input for present and future robotic space exploration missions.

For the LIBS measurements, a commercial handheld LIBS instrument was used (details in Section 2). In recent studies, the same type of instrument was used to analyze collected geological samples in laboratories where promising outcomes for mineral identification and elemental quantification were reported relying on statistical as well as on analytical approaches [32–36]. One group also reported first tests from a volcanic field-site in New Mexico, USA [37]. A recent review gives an overview of the growing product range of handheld LIBS instruments and studies using these [38]. Most presented studies focus on the evaluation of quantification accuracies on samples measured in a laboratory setting which is a crucial factor for the performance of LIBS instruments. However, in this work we evaluate the performance of such a commercial handheld LIBS instrument directly in the field without the purpose of reporting quantitative results. We analyzed the natural surface in

its original environment, which poses additional challenges compared to measurements in the laboratory. Experimental parameters such as the sampling distance and the angle of incidence of the laser can be fixed in laboratory measurements which usually improves the performance of LIBS measurements. Moreover, while it is an advantage of LIBS that sample preparation is not necessarily needed, samples with, for example, ideally flat surfaces can be prepared for laboratory LIBS investigations for improved LIBS measurements [22]. In the field, however, ideal positioning of the used handheld LIBS instrument is not always possible and affects the collected data.

The focus of this study is to analyze the performance of a commercial handheld LIBS device in a field setting and to identify the associated challenges compared with laboratory studies. We first present methods to validate our approach using a laboratory study simulating varying distances between the instrument and sample. We then discuss our LIBS data acquired at a field site on the island Vulcano characterised by layered volcanic ash. A PCA analysis was then performed on this dataset as a first data exploration method followed by a detailed layer-by-layer investigation of the observed elemental emission line intensities with respect to the expected mineralogy of the outcrop. Even though the LIBS spectral characteristics depend on the specific experimental parameters and local ambient conditions, our results provide general and practical considerations for both terrestrial and extraterrestrial applications such as by robotic platforms or for human in-situ exploration of the Moon [39], where astronauts could be equipped with a handheld LIBS instrument to analyze the geochemical composition of lunar rocks and regolith.

2. Instrumentation and method

2.1. LIBS handheld device and method

For the field measurements, a commercial portable handheld LIBS instrument, namely a Sci-Aps Z-300, was used. The instrument uses a Nd:YAG laser operated at its fundamental wavelength of 1064 nm with a repetition rate of 10 Hz and a laser energy of 5-6 mJ per pulse. The focused laser beam size is in the order of 50 μm. A wide spectral range of 190-950 nm is covered by three spectrometers which are equipped with charge-coupled devices (CCD).A detailed description of the predecessor model Z-500 can be found in [32]. The difference lies only in the smaller spectral range of the Z-300, as compared to the Z-500. The wavelength calibration is done internally by the instrument by pointing the laser to a metal plate inside the instrument when the instrument is switched on. This calibration needs to be repeated after a fixed time interval which was set to 30 min in our case, to account for changing conditions such as the instrument's inner temperature. The volume in which the LIBS plasma evolves is kept under a constant Ar flow of 12 psi during the measurement because emission line intensities are usually stronger in Ar atmosphere than in ambient (terrestrial) conditions [40, 41]. The LIBS plasma, and therefore its emission characteristics, depend on the atmospheric pressure and gas composition where physical properties of the gases such as the ionization energy and the heat capacity are important factors [42]. This is a critical aspect to consider when planning a LIBS instrument for planetary exploration as other planetary bodies have different atmospheric conditions from Earth, resulting in different LIBS plasma characteristics [16]. With regards to Ar, its physical properties are beneficial for LIBS analysis com-

pared to terrestrial conditions as discussed in detail by [40]. Furthermore, the LIBS plasma in Ar atmosphere has a nearly uniform distribution of temperature and electron density which reduces the effect of self-absorption and emission line shifts [43]. However, it is important to point out that the use of Ar results in the emission lines of Ar appearing in the LIBS spectra. Atmospheric emission lines are common in LIBS data obtained in non-vacuum conditions as species from the atmosphere contribute to the plasma, such as carbon emission from a Martian atmosphere [44], or nitrogen in LIBS spectra obtained in terrestrial conditions.

A single measurement with the handheld LIBS instrument consists of a raster with multiple ablation points. For this field study and the laboratory study (see Section 2.3), a 3×4 raster was selected in which the distance between the outer borders of individual craters is $\approx 40\,\mu$m. At each point, five successive laser pulses are done, but only the radiation from the last three induced plasmas is recorded. The first two laser pulses are called "cleaning shots" as the shock-wave of the LIBS plasma removes dust or superficial contamination from the sample and thin layers (e.g. from weathering) are ablated. The detector measures the radiation from each plasma starting after a delay of 630 ns after the laser pulse and during an integration time of 1 ms. The described settings of timing, size of the raster, and number of laser pulses can be changed, however, we measured all samples with the same settings for a better comparability. The measured spectra of each individual point in the raster, except for the cleaning shots, is accumulated and from the whole raster, an average spectrum is obtained.

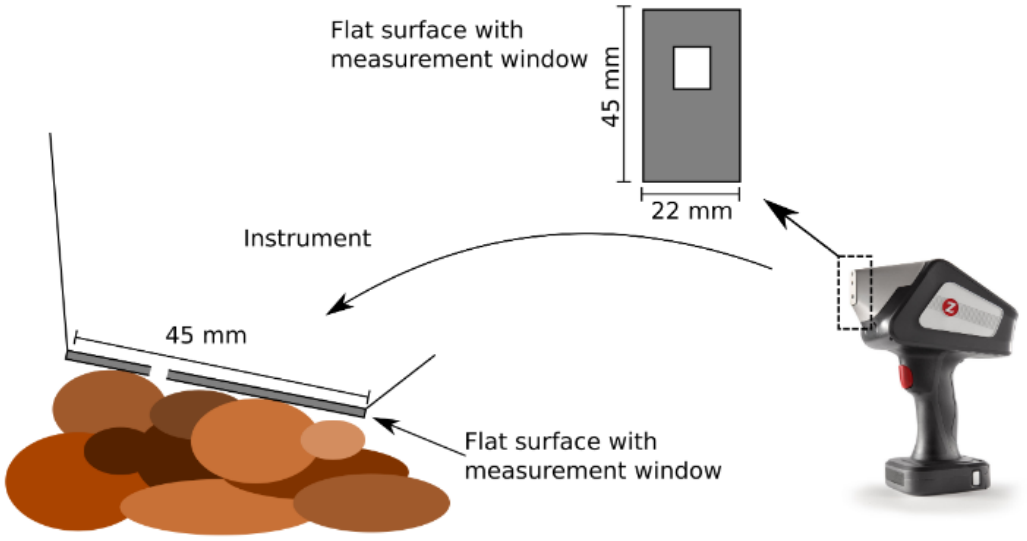


Figure 1: Illustration of one of the major challenges for LIBS field measurements with the handheld device: surfaces that are not flat on the scale of the instrument's contact flat surface ($45 \times 22\,\mathrm{mm}^2$) can not be measured with a direct contact between the instrument and the sample. As a consequence, the distances can vary in the range of a few centimeters.

2.2. Application in the field

As the measurements were performed in the field it was not possible to keep the experimental conditions as constant and ideal as in a controlled experiment in the laboratory. The experimental parameters that were changing the most in the field were the instrument distance to the sample, the angle of incidence of the laser radiation on the naturally rough surfaces and the angle under which the plasma radiation is collected. The analysis window of the instrument is located in a flat surface with an area of size $2.2 \times 4.5\,\mathrm{cm}^2$ which should be placed in contact to the ideally flat sample surface for optimal data acquisition. If the contact between the instrument and the sample's surface is not well accomplished, the sampling area might not be in the best focus position for the most effective material ablation. This was frequently the case for the samples analyzed in the field and a sketch illustrating this situation is shown in Figure 1. The encountered natural surfaces on Vulcano were often rough on scales much smaller than the flat area of the instrument and therefore challenging to measure with the handheld LIBS device. This led to LIBS spectra acquired with varying distances on the scale of millimeters up to a few centimeters between the sample surface and the instrument. Related to variations in the sampling distance is the contribution of Ar atoms to the LIBS plasma from the introduced Ar atmosphere as it can change depending on where the breakdown takes place. Another experimental parameter that was changing in the field was the surrounding temperature which does not affect the LIBS plasma itself but can slightly change the detection geometry and therefore the wavelength calibration. Consequently, recalibration of the wavelength was done regularly.

During the data analysis some spectra showed strong emission lines of Ar and contain almost no signals from other elements. The presence of Ar emissions in the spectra was expected but not the relatively strong impact on the spectra quality. In such cases, it is most likely that the distance to the sample was too large to create the LIBS plasma on the surface of the sample and the breakdown was almost completely in the Ar atmosphere. These spectra provide no relevant information about the geochemistry of the investigated samples and were therefore rejected from further analysis. An example of such a spectrum is shown in Figure 2 *(top)* where strong Ar emission lines in the spectral range above 650 nm (marked with dashed line) can be seen. During the measurement campaign, it was difficult to control the exact distance to the sample and hence the quality of the LIBS spectra. An automated procedure to identify and remove these primarily Ar spectra was applied after data collection. The procedure relies on summing the counts in the spectral ranges below and above 650 nm, respectively. All Ar emission lines are in the spectral range above 650 nm and if the ratio of the summed counts above and below is larger than one, the spectrum was rejected. With this approach, $\approx 14\,\%$ of the spectra, 8 out of 57 spectra, were rejected. An example for a spectrum which was not rejected and contains relevant geochemical information is shown in Figure 2 *(bottom)*.

2.3. Laboratory study: effect of varying distance

As the distance of the instrument to the sample was found to strongly influence the quality of the LIBS data, a laboratory experiment was performed to investigate how this affects in particular the Ar emission. A gypsum ($CaSO_4$ x $2\,H_2O$) pellet was chosen as the target sample for its homogeneity

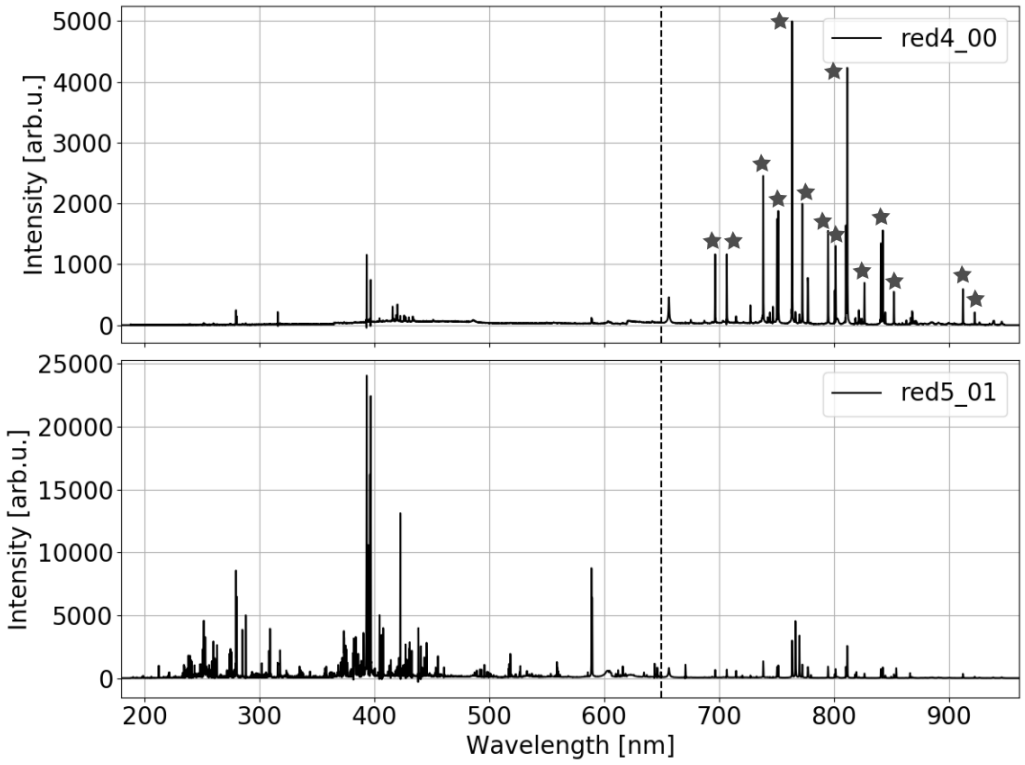


Figure 2: *Top*: Example of a spectrum with strong Ar emission lines (marked with stars) and with almost no other information. The total intensity of this spectrum is dominated by emission lines above 650 nm (dashed line). The ratio of the integrated intensities above and below 650 nm is larger than one and the spectrum was rejected from further analysis. *Bottom*: Example of a good quality spectrum with stronger emission lines in the spectral range below 650 nm than above this wavelength. This spectrum contains information about the elemental composition of the target and has a ratio of integrated intensities above and below 650 nm smaller than one.

and simple sample matrix structure. This allows to relate changes in the Ar emission mainly to the change in distance and reasons the choice of sample which is not motivated by expected minerals at the measurement site in the field. For the experiment, the instrument was fixed and the sample was mounted on a stage. The height of the stage was changed from a position where the instrument and the sample were in direct contact to a position where the distance was ≈ 40 mm. At five different intermediate positions, five measurements were performed, respectively. Several neutral and one ionic Ca emission lines were chosen for the analysis. All Ar emission lines in the data were identified to come from only neutral Ar. Two moderately intense and free standing Ar lines, one close to 700 nm and one Ar line near the end of the spectral range beyond 900 nm were selected for analysis. All emission lines were fitted with Lorentzian line shapes in each of the five spectra per position and the intensities were averaged. In Figure 3, the intensities of the Ar and Ca emission lines are shown for increasing distance between the sample and the instrument, and different trends of the Ca and the Ar emission lines can be observed. The emission lines of Ca(I) and Ca(II), which come from the sample matrix, are overall decreasing with increasing distances. However, the Ca (I) emission lines show a small increase from 0 mm distance to 10 mm distance, which is not observable for the Ca (II) emission line. Furthermore, the Ca (II) drops more strongly than the Ca (I) intensities after the distance of 20 mm. This indicates that the plasmas at larger distances have lower temperatures since ionized species are more abundantly present and excited in high temperature plasmas. In contrast to the Ca emissions, the intensities of Ar atoms emission lines show an increase until a distance of 20 mm and

then decrease for larger distances. This suggests that a distance of 20 mm to the sample is optimal for Ar emission, while the emission of components coming from the sample is reduced.

When comparing the ratio of the integrated intensities above and below 650 nm, as was also done for the field data, the ratio is only larger than or close to one for the instrument-sample distance of 40 mm. However, the spectra at this distance are already of a bad quality and the reason for the comparatively small ratio can be found in the characteristics of the LIBS spectrum of the gypsum sample. Gypsum has a large concentration of Ca ($\approx 23\,\mathrm{wt}\,\%$) which is most likely larger than in the ash layers measured on Vulcano. Furthermore, Ca lines tend to be strong already at small concentrations which is not the case for most other elements. With the gypsum sample, the integrated intensity below 650 nm is larger than it would be for samples with lower Ca abundances. Additionally, the emissions of Ca as well as O above 650 nm contribute to the sum of the range with the Ar emission lines. Thus, with such samples, the ratio at which a spectrum should be rejected should be chosen to be much smaller. With a threshold ratio of 0.4, all spectra measured at 40 mm distance, and almost all at 30 mm, would be rejected with the discussed approach.

This laboratory study further shows that the Ar emission is not suited to compensate for effects of varying sampling distances as the emissions coming from elements in the sample (here: Ca) and the Ar emissions behave in different ways. Similar results regarding the contribution of C emission from a simulated martian atmosphere to LIBS plasmas were shown in [44] for other varying experimental conditions, such as varying laser irradiance or varying

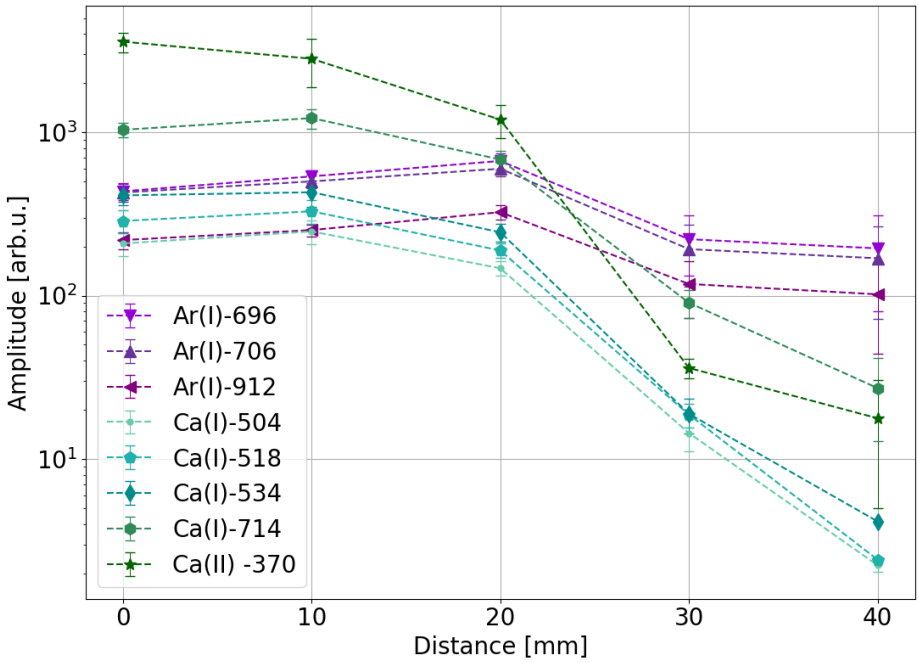


Figure 3: Fitted intensities of Ar and Ca emission lines for increasing distances between the sample and the instrument. The error bars indicate the standard deviation of five measurements. The Ar emissions coming from the atmosphere show a slight increase followed by a decrease while the Ca emissions decrease only with increasing distance.

grain sizes.

2.4. Data pre-processing

Prior to the actual data analysis, LIBS data needs to be pre-processed [25] and particularly for the spectra in this study, which were measured at varying distances, a dedicated data treatment is essential. Different approaches for data normalization were tested and evaluated. In the literature, it is suggested that normalization to Ar emission lines contributing from the atmosphere can improve univariate calibration curves [41]. Our laboratory study

with varying sampling distances (Section 2.3) showed, however, that the Ar emissions are not suitable for normalization of our data. Despite having rejected the spectra with the strongest Ar contributions, when normalizing to the total emission intensity the PCA outcomes were strongly influenced by the Ar emissions, which was observed in the PCA loadings. Variance in the data due to the elements of the samples remained mostly hidden with this approach. A similar result was obtained when normalizing to the maximum intensity of the spectrum. In order to avoid this strong influence of the non-analytical Ar emission lines on the PCA, they were masked in the spectra. All Ar emission lines in the present spectral range were thus replaced by the average of the two values at the borders of the corresponding emission line ranges. A list of all masked Ar emission lines can be found in Table 1. This approach seemed most suitable for our objective to study the geochemical variations and elemental trends in the ash layers with PCA. After all observed Ar emission lines were masked, the integrated emission intensity of each spectrum was used for normalization. In a further step the spectra were mean centered and divided by their standard deviation before PCA so that all spectra have a mean value of zero and a standard deviation of one.

3. Investigation of volcanic deposits - description and LIBS results

3.1. Description of the outcrop

The island of Vulcano (Aeolian Islands, Sicily Italy) consists of several volcanic edifices whose formation overlapped in time and space ([27] and references therein). One of the most recent areas of volcanic activity is the northern peninsula Vulcanello composed of a basal lava platform (1.9 ka) super-

Table 1: Ar (I) emission lines as listed in the NIST database [45] that were masked in the spectra in order to suppress their influence on the analysis. Also shown are the ranges in which values were replaced by the average of the two values at the end and the beginning of the range.

λ (NIST) [nm]	masked range [nm]
696.5	695.6 - 697.5
706.7	705.7 - 707.7
727.3	726.0 - 728.5
738.4	737.3 - 739.6
750.4; 751.5	749.4 - 752.7
763.5	762.1 - 764.9
772.4; 772.4	771.5 - 773.3
794.8	793.8 - 795.8
800.6; 801.5	798.6 - 803.6
810.4; 811.5	808.9 - 813.4
826.5	825.6 - 827.4
841.8; 842.5	839.9 - 843.7
852.1	851.3 - 852.9
912.3	911.4 - 913.3
922.5	921.7 - 923.1

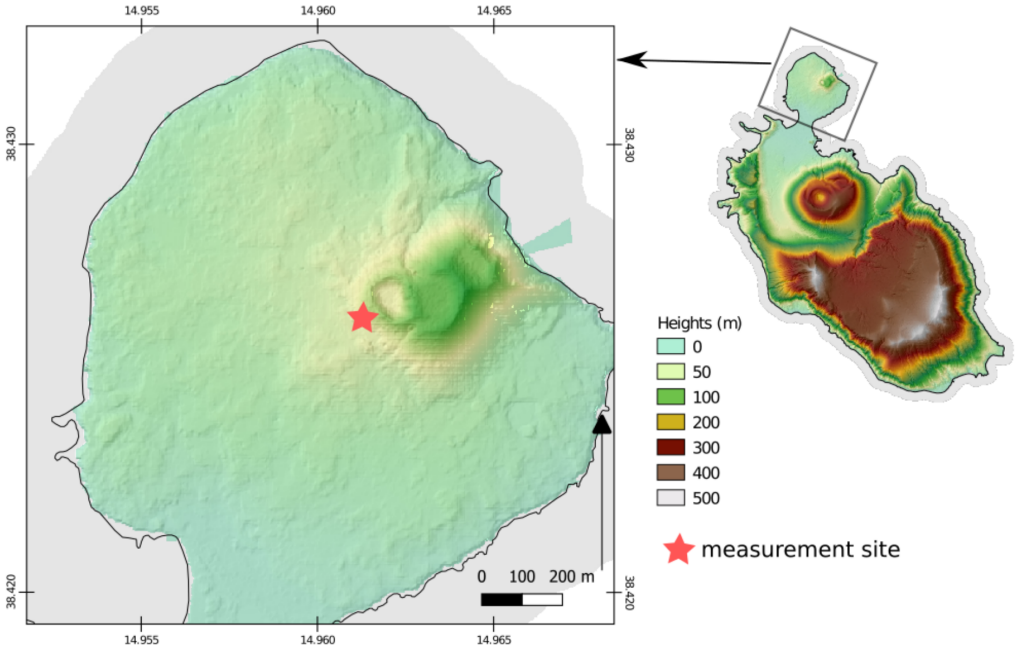


Figure 4: Map of Vulcano showing a detailed inset of the northern peninsula and Vulcanello. The star symbol marks the outcrop location of this study.

imposed by three partially overlapping scoria cones (0.4 ka) aligned NE–SW along the northern ring fault of the La Fossa caldera [27]. An overview map of Vulcano with a detailed view of Vulcanello is shown in Figure 4. Vulcanello mostly erupted alkali-rich shoshonitic products with a few latitic products characterizing the last cycle of activity [46]. The outcrop investigated in this study is located at the foot of the southernmost cone, which is considered to be the youngest and is dominated by pyroclastic deposits [27]. These are composed of a several meters thick thinly bedded, vesciculated and multi-colored ashes and lapilli of the $vu3_b$ member of the Vulcanello formation [47]. A detailed image of the outcrop is shown in Figure 5 *(a)*.

As described in Section 2, one LIBS measurement in this study consists of

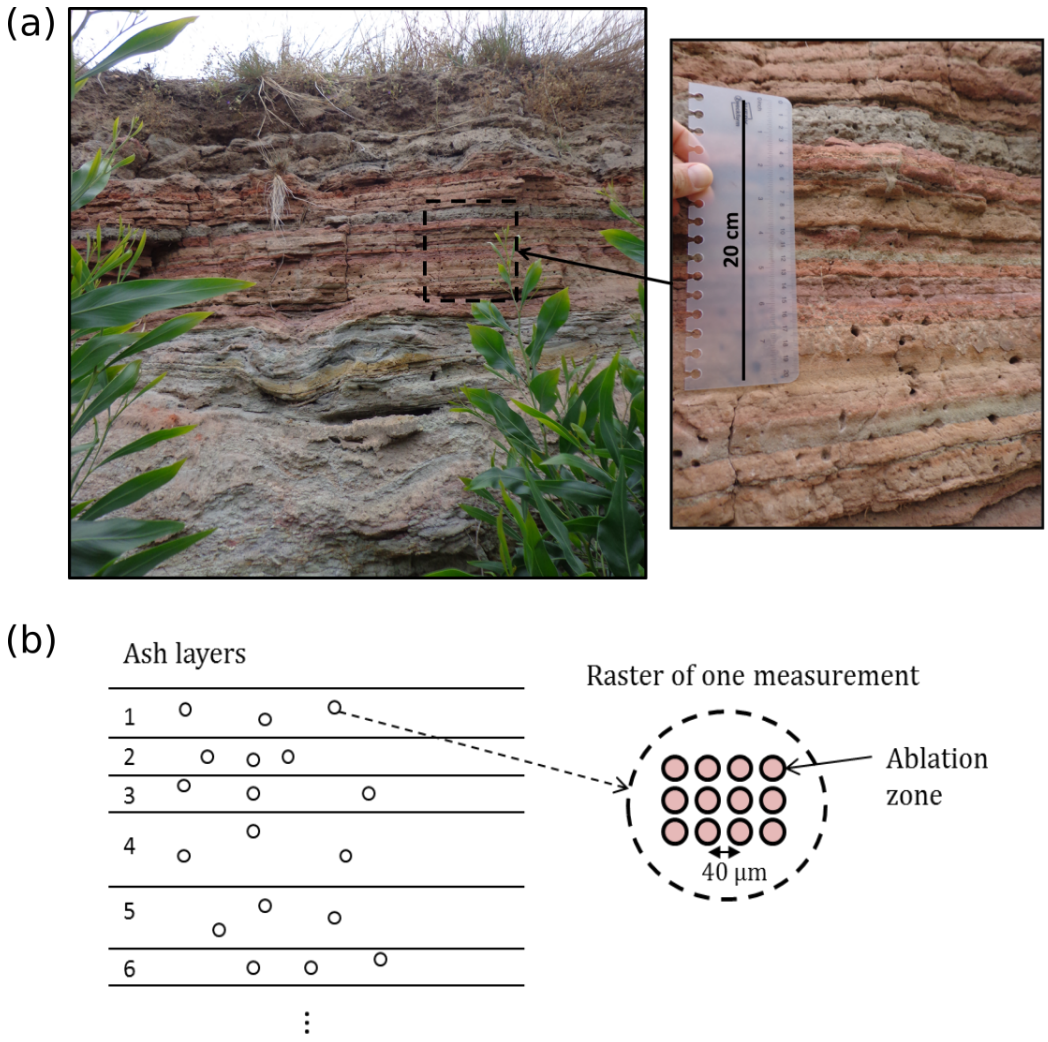


Figure 5: *(a)* Image showing the investigated outcrop on Vulcanello with layers of differently colored volcanic ashes. The dashed black box marks the area that can be see in the zoom *right*. The layers not only differ in color, some of them are hard rocky surfaces while the majority consists of loose, poorly consolidated material. *(b)* Schematic drawing of measurement procedure. In each layer, three different locations were measured while at each position material was ablated in a raster of 3×4 positions.

a raster with 12 ablation zones in total. A schematic drawing of the measurement procedure for the investigated ash layers can be seen in Figure 5 *(b)*. In each layer, three LIBS measurements were acquired and in total, 19 layers were investigated of which the uppermost layers can be seen in the zoom in Figure 5 *(a)*. For a better traceability, we assigned numbers to the layers from top to bottom along with a color code of "gray", "red", "orange", or "yellow" based on our visual inspection. Repeated colors were numbered as well. A list of the labeled layers is provided in Table 2 and can be used for comparison with the image of the outcrop in Figure 5 *(a)*. Not only the colors of the layers change but also their physical appearance as some layers appear harder while others are more brittle and less robust in comparison, and some even crumbled during the measurement. This is an additional aspect that needs to be considered in the LIBS analysis since the quality of a spectrum is influenced by the laser-matter interaction and how well the laser couples to the sample mainly depends on the physical matrix of the sample. In general, harder and more consolidated materials produce better LIBS spectra while loose materials and even soils are more difficult to analyze with LIBS.

3.2. LIBS spectra

For a first overview of the data, the average and in some cases single LIBS spectra are shown for each layer in Figure 6. The spectra are presented in the order of the layers from top to bottom and their colors correspond to the assigned layer color. In these spectra, the Ar emission lines were not masked as described in Section 2.4 to emphasize that they are present in all spectra with variable intensities. For each layer, n gives the number of spectra and some intervals with strong emission lines of Si, Mg, Al, Ca, Fe, Na, CaF, H,

Table 2: Naming of the layers from top to bottom. The first (top) layer is layer 1 and has the name gray 1 while the last (bottom) measured layer is gray 6.

Layer	Naming	Layer	Naming
1	gray 1	11	yellow 2
2	red 1	12	orange 3
3	orange 1	13	gray 4
4	gray 2	14	orange 4
5	yellow 1	15	orange 5
6	red 2	16	red 5
7	gray 3	17	gray 5
8	red 3	18	yellow 3
9	red 4	19	gray 6
10	orange 2		

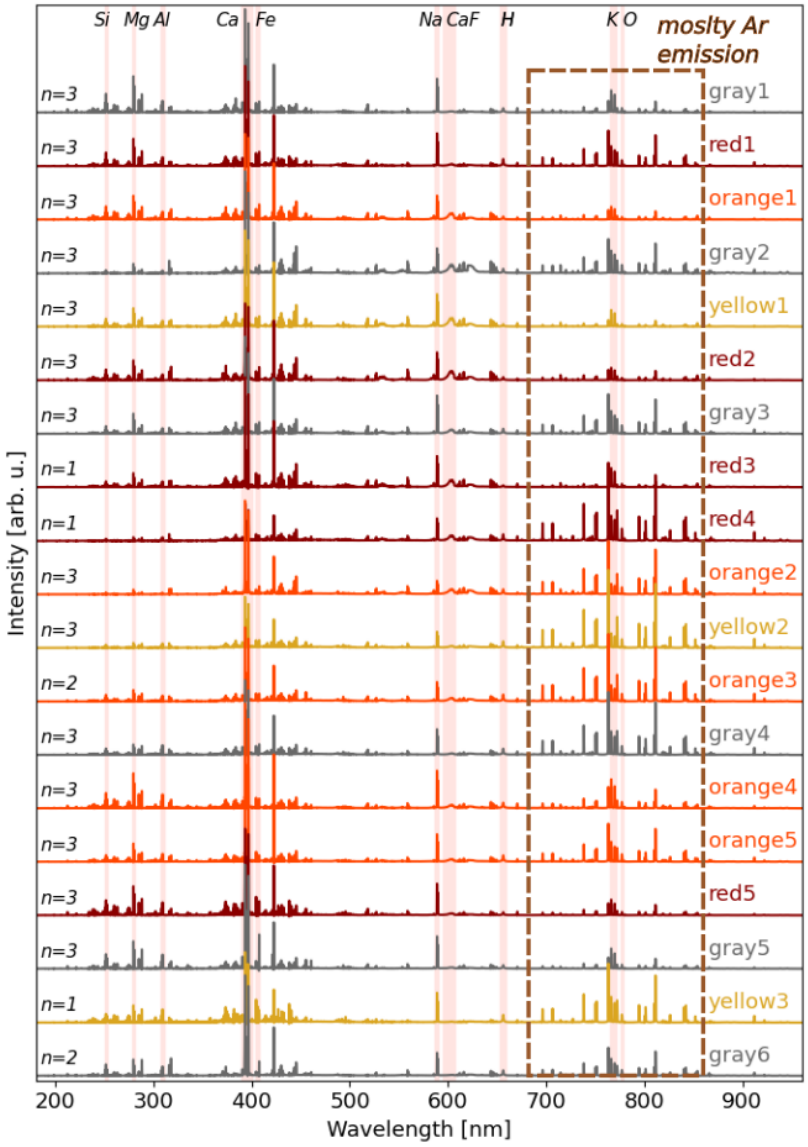


Figure 6: Mean spectra or single spectrum of each layer in the order from top to bottom to be compared with Figure 5. Here, the spectra were normalized by their total emission intensity but the Ar emission lines in the spectral range > 650 nm were not masked in order to visualize their influence. For each layer n indicates the number of available spectra that were averaged if $n > 1$. Spectral ranges of Si, Mg, Al, Ca, Fe, Na, CaF, H, K, and O emissions are marked in light red.

K, and O were marked in light red but clearly each spectrum contains more emission lines which could not all be marked in this representation.

3.3. Data exploration - PCA

In order to explore the data and to investigate chemical variations of the different ash layers, a PCA was performed with the LIBS spectra that fulfilled our quality criterion. In Figure 7, the PC 1/PC 2, PC 3/PC 4, and PC 5/PC 6 score plots are shown. For each PC, the explained variance in the data by the particular PC is given in brackets. The accumulated sum of the explained variance up to PC 6 is 89.9 %. This indicates that the variance in the dataset is distributed over multiple spectral features, as 10 PCs (not shown here) are needed to explain more than 95 % of variance in the data. Furthermore, for interpretation and discussion of the PCA, the loadings of PC 1-6 are given in Figure 8. The loadings indicate correlations between the PCs and spectral features, and thus how large the influence of these spectral features on the particular PC is.

In general, regarding the score plots in Figure 7, where the score value of a spectrum is colored by the color of the corresponding layer obtained from visual inspection, no clustering or trend due to the layer color is observable. However, colors ascribed to the layers are qualitatively and subjective. For individual layers, which are represented by symbols in the score plots (Figure 7), similar trends for all spectra from the same layer can be seen in some cases. For example, the scores of layer *red5* are relatively close to each other in all three score plots. Furthermore, there are also cases where the scores of two spectra from one layer are very similar and plot close together while the third one has score values rather different from the others and plots further

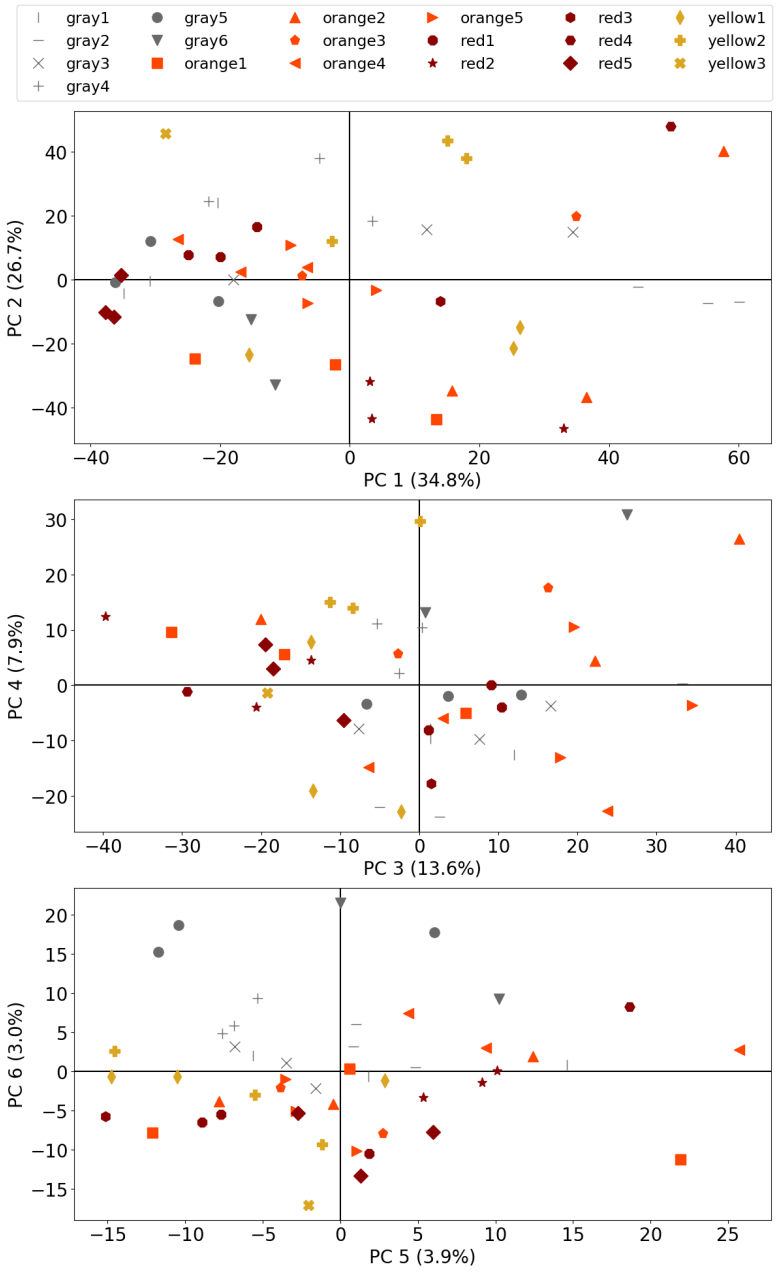


Figure 7: Score plots of PC 1/PC 2, PC 3/PC 4, and PC 5/PC 6 where the number in brackets is the explained variance of the dataset by each component. The colors correspond to the color of the layer attributed from visual inspection while the symbol indicates individual layers. There is no distinct grouping according to layer color observable, but for some individual layers consistent trends for spectra from the same layer can be seen.

away, see for example the scores of layer *yellow1*. In general, these trends are promising as they allow to observe elemental variations among the layers and to evaluate the homogeneity of the layers as well as the reproducibility of the measurements. Larger distances between score values of spectra from the same layer can serve as an indication for the two latter mentioned factors. However, besides the occasionally observable trends, a clear clustering due to the individual layers is not observable. One reason for this can be the already discussed not well controllable distance between the sample and the instrument which introduces variations among the spectra of one layer. To reduce those experimental influences as seen in this analysis and to increase high quality data per layer it would be worthwhile to analyze more positions per layer in future geochemical field investigations with such a handheld LIBS device. In the following, we discuss briefly the observations from the PCA to reveal correlations and give interpretations on the score values and the loadings.

First, the loadings of PC 1 mainly distinguish between spectra with rather strong emission signals of Ca, K, and O as well as molecular emission bands of CaF and spectra with relatively strong emission lines of Al, Si, Mg, and Na. Molecular emission bands, as those of CaF, can serve as an indirect detection of elements which are otherwise challenging to detect in the used spectral range (200-900 nm) such as Cl and F [48–50]. For the Ca emission lines, the neutral and single ionized lines behave differently. The neutral Ca emission lines emit in a spectral range larger than 400 nm and have positive correlations with PC 1. On the other hand, the ionized Ca emission lines are in the spectral range below 400 nm and show only small correlations

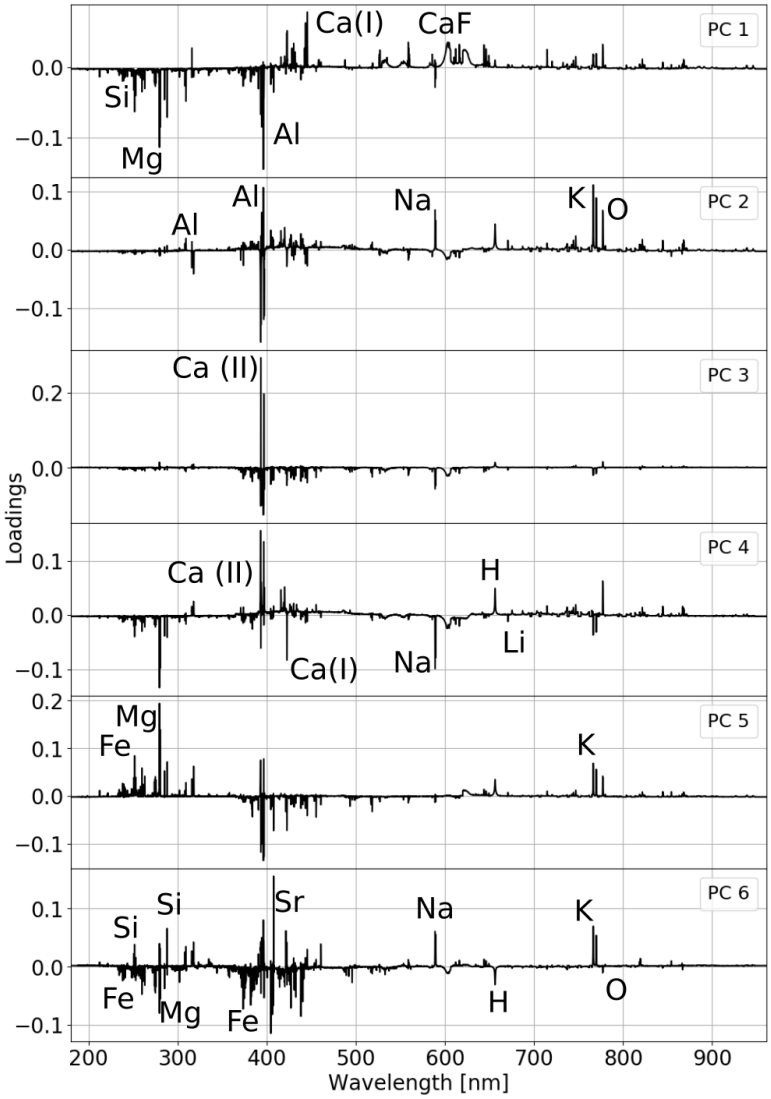


Figure 8: Loadings of PC 1-PC 6. Positive values indicate a positive correlation with the PCs resulting in positive score values of spectra which have features at these particular positions. For negative loadings the opposite applies. For clarity, annotations of the elements were not done for each PC. For some Ca features, the ionization state was given as anti-correlations of neutral and first ionized Ca emissions were observed.

with PC 1 that are overall negative, except for the Ca (II) line at 315.9 nm. One reason for this difference could be changing plasma conditions, such as different plasma temperatures and electron densities that favor either neutral or ionized Ca emission. But also the varying distance could be responsible as slightly different trends with distance were observed for neutral and ionized Ca emission lines in the laboratory study discussed in Section 2.3. A zoom of the loadings of the 6 PCs to the spectral range 390-400 nm where two Al (I) and two Ca (II) can be found is shown in Figure 9. The dashed lines mark the expected center positions of the emission lines and differences in the emission line shapes and positions are observable for all PCs. These changes could be caused by self-absorption or line shifts. Self-absorption is an effect where highly abundant elements emit photons in the hot plasma core which are reabsorbed by atoms of the same element in the colder outer plasma regions. This can lead to more broadened emission lines and even dips in the center of emission lines [19, 7]. Line shifts can occur because of different surrounding pressure conditions [51] but also because of instrumental factors such as the collection angle (sub-optimal positioning of the instrument can lead to aberrations) or the repeated wavelength calibration that was necessary due to the heat. For PC 1 the observed shapes of the Ca (II) emission lines are most likely a result of different degrees of self-absorption. Stronger self-absorbed lines have more extended wings which show a negative correlation with PC 1. To conclude, it is challenging in particular for the Ca (II) emission to derive interpretations related to abundances in the layers as these lines show influences of plasma as well as instrumental conditions.

PC 2 has the largest positive correlations with Al, Na, H, K, and O emis-

sion lines, which can indicate the presence of alkali-rich feldspars in layers which high score values on factor 2. On the other hand, negative correlations are mainly observed for Ca emissions, neutrals and first ionized ones.

PC 3 shows the strongest positive correlation with the usually strongest Ca (II) emission lines at 393.4 nm and 396.8 nm, see Figure 9. Narrow Ca (II) lines have a positive correlation while broader, most likely self-absorbed, emission lines have a negative correlation with PC 3. Other positive correlations are observed for H and O emission lines but much smaller than the narrow Ca (II) emission lines.

PC 4 reveals a strong influence of Mg, Na, and Ca (I) emission lines resulting in negative score values for spectra that exhibit these features. On the other hand, stronger H and O features lead to positive score values on PC 4. Ca (II) emission lines reveal an influence of the line position of the two strongest ones on PC 4, see Figure 9.

PC 5 mainly separates spectra with somewhat stronger emission lines of Fe, Si, Mg, and K from those with Ca features. For this PC, a further inconsistent observation can be made for neutral Al emission lines, as the lines at 308.2 nm and 309.3 nm have a positive correlation with PC 5 while the ones at 394.4 nm and 396.2 nm have a negative one. This means, as already seen for Ca emissions, that no relative quantitative conclusions from PC 5 can be made for Al concentrations in the layers.

PC 6, finally, has positive correlations with emission lines of the alkalis Na and K as well as with Si and is the first PC that shows clear Sr emission lines. Negative correlations are observable mainly for Fe and Mg emissions. Especially, the influence of Fe is higher on PC 6 than on all other previous

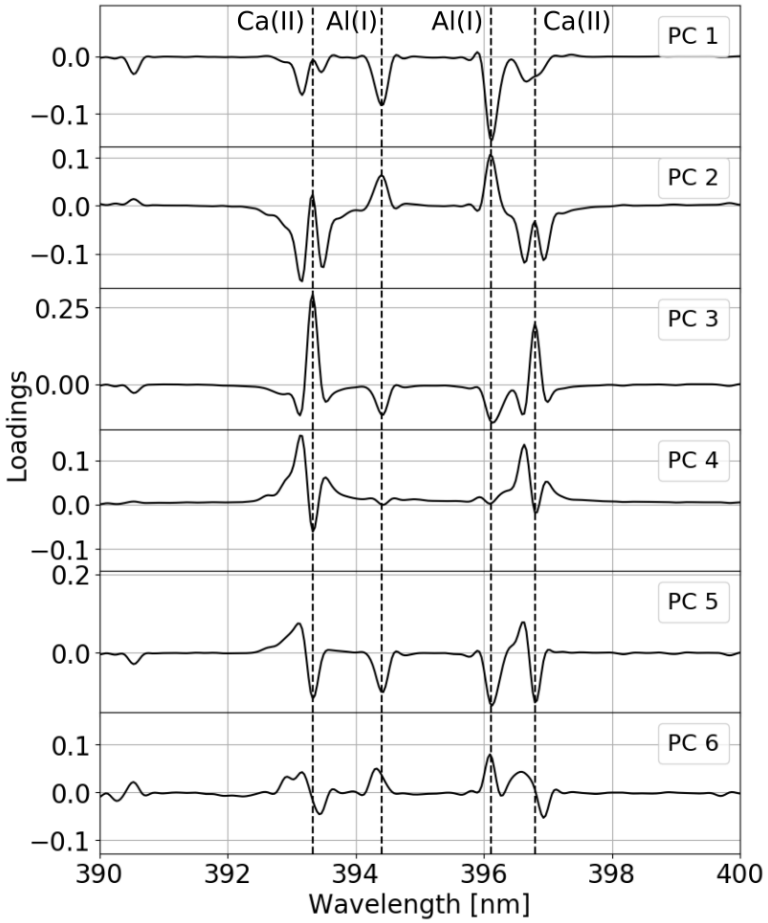


Figure 9: Same plot of the loadings as in Figure 8 but zoomed to the spectral range 390-400 nm in order to better visualize the different line shapes of the Ca (II) emission lines in the loadings. Line shapes that show not only changing peak heights but dips or zero crossings indicate that not only the intensity of the particular element has an influence on the PC. Effects that contribute to those line shapes can be, for example, shifts in the line position due to experimental conditions or self absorption of emission lines.

discussed PCs. The PC 5/PC 6 score plot in Figure 7, reveals the only but also slight trend due to color. Almost all spectra from layers considered as gray have positive score values on PC 6. Thus, red, orange, and yellow layers are expected to have higher Fe abundances than gray layers. The reason could be the presence of Fe-oxides which are responsible for reddish colors.

To summarize the observations from the PCA, clustering was observed for several individual layers but not between layers due to the color label. The results are promising as some trends according to individual layers became apparent. Furthermore, the loadings indicate influences of different elemental combinations and allow therefore to make relative predictions of elemental abundances from the spectra. Nevertheless, these predictions are challenging for elements whose emission lines show influences of line shape and line position in the loadings as observed mainly for Ca (II) in this analysis.

3.4. Layer-by-layer analysis

In addition to the PCA, a layer-by-layer analysis using univariate fits of several emission lines was done. Emission lines of major as well as minor and trace elements were fitted with Lorentzian curves. Besides the emission line fits, the intensity of the CaF molecular emission band was tracked by integrating the measured intensity in the interval 602-603.5 nm. For Ca, an emission line at 714 nm was selected which is less self-absorbed than the strong Ca (II) lines slightly below 400 nm. All results are shown in Figure 10 as single points which are at maximum three fits for one layer. The order from left to right in the plot corresponds to the order top to bottom of the outcrop. The dashed line connects the mean values of the shown fits. In some cases, the fits of one layer show a large scatter around the mean

value, but in other cases the fitted intensities are unambiguous, which is in agreement with observations made in the PCA, see Section 3.3. The objective of this analysis is to investigate elemental correlations among the layer and possible depositional trends. Mostly major elements were discussed in the PCA analysis while in this univariate approach minor elements that often have only a few emission lines in the commonly used spectral range (200-900 m) can be included.

Similar to the PCA, no distinct trend of element abundances related to color is observable. Nevertheless, except for the one spectrum of layer *red4*, the red layers are relatively enriched in Fe whose oxides are responsible for reddish colors. Regarding correlations between emission line intensities, a distinct correlation between the Al (I) and the Si (I) emission lines is visible in Figure 10, which is confirmed by a high Pearson correlation coefficient of 0.97 among the measurements. Such a correlation is characteristic of products of volcanic origin. Additional but somewhat weaker correlations are observable for the alkaline elements Na and K but also for Mg and Fe which are typical elements of mafic rocks. The only clear anti-correlations according to Pearson correlations are found for the Ca (I) emission line with Al(I), Si (I), Fe(I), and Mg(I) line intensities. This is mostly in agreement with the loadings of PC 1 discussed in the previous section as those indicate an anti-correlation of Ca with almost all other elements, see upper plot in Figure 8. In general, the observed correlations are in agreement with the description of the ashes in [47]: The erupted lava is dominated by alkali rich shoshonitic products which are igneous K-rich basaltic trachyandesites containing alkali feldspars, olivines and pyroxene. Thus, the ashes are composed

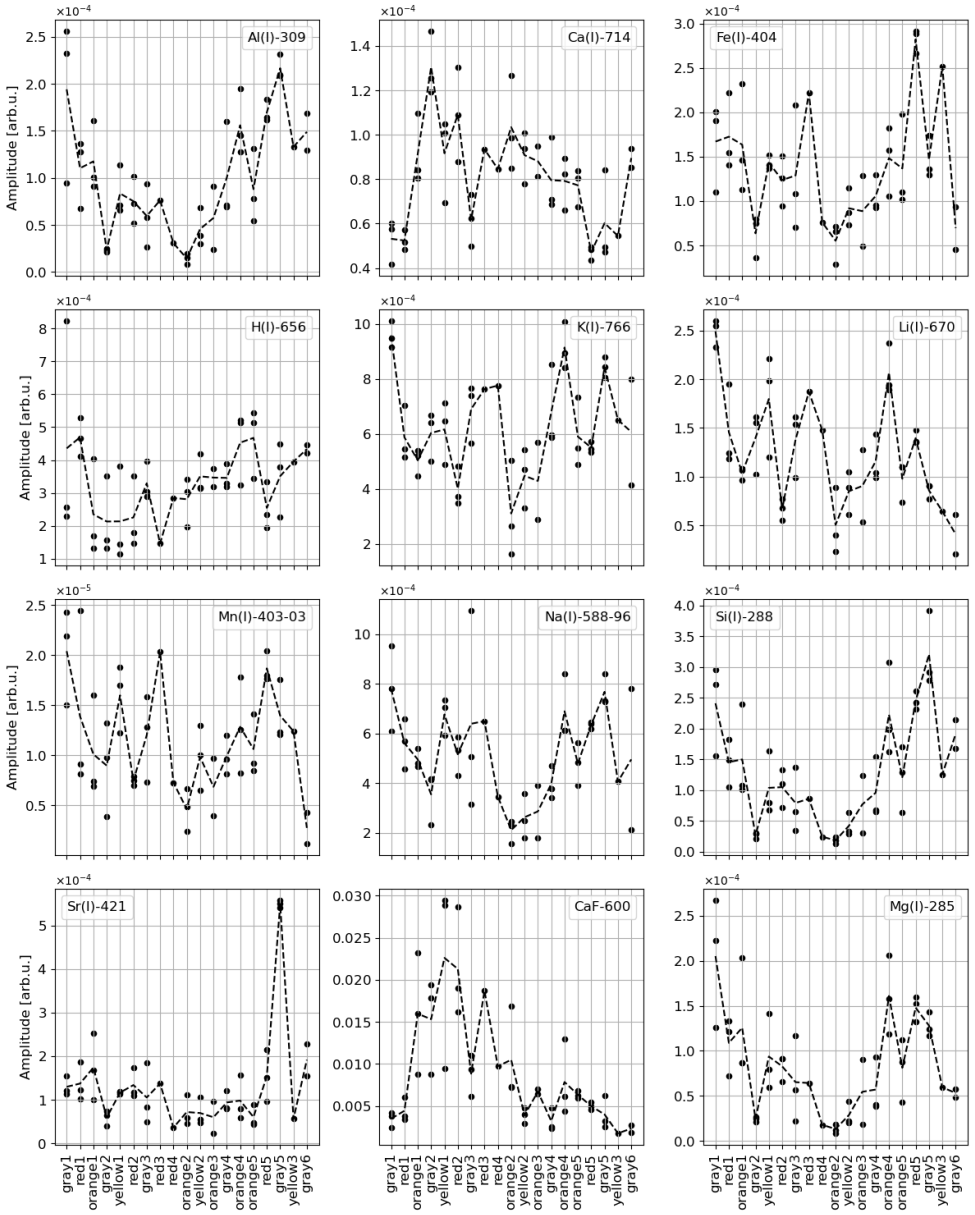


Figure 10: Emission lines of Al, Ca, Fe, H, K, Li, Mn, Na, Si, Sr, and Mg were fitted with Lorentzian curves and the results are shown here for the layers from top to bottom. The intensity of the CaF molecular band are integrated intensities in the range 602-603.5 nm. All results from the available spectra are shown while the dashed line connects the mean values of each layer.

of felsic and mafic minerals with high alkaline and low Ca contributions. Especially, the observed anti-correlation of Ca with all other elements confirms the shoshonite-alkaline character of these igneous materials.

For the minor and trace elements, the strong Sr signal for layer *gray5* in all three spectra is particularly noticeable. This observation can be compared with the PCA in Section 3.3 as Sr emissions were identified to have a positive correlation with PC 6. Indeed, all three spectra from layer *gray5* have large positive score values on PC 6. Besides this strong Sr emission in this layer, similar trends of the Sr emission line among the layers could be identified with Al, Na, and Si emission lines. The Mn emission line has the strongest correlation with the Fe emission line (Pearson correlation of 0.79) which can be an indication for redox processes. But Mn has furthermore positive correlations with the alkaline metals Li, Na, and K as well as with Mg. Similar observations can be made for the Li emission line, which has besides the correlation with the Mn emission, correlations with the lines of K, Na, and Mg. The intensities of H and CaF are variable among the layers. The H emission is known to be strongly influenced by matrix effects and experimental conditions most likely due to its low atomic mass and behave differently than heavier elements in the LIBS plasma [52, 44]. Thus, quantitative conclusions can only be made with care, especially with the rather loose materials in this investigation. However, the lower part of the outcrop seems to be overall more hydrated than the upper part. The CaF molecular intensity cannot be related directly to F abundances [53] as the CaF molecules form temporarily in the plasma and their concentration depends also on Ca abundances. Nevertheless, the band intensity can be used for

estimates of the F concentration in the layers and a slight increase of the CaF signal after the second layer *red1* is observable followed by an decrease after layer *red4*. A similar trend can be seen for the score values on PC 1, which has the largest positive correlations with Ca (I) emission lines, indicating that there was enough Ca present in these layers in between to form CaF molecules in the LIBS plasma. Thus, these layers might have higher abundances of F containing minerals such as fluorite (CaF_2) or fluorapatite ($Ca_5F(PO_4)_3$). Indeed, the CaF band intensity is the only feature that has a positive Pearson correlation (0.65) with the Ca (I) emission line.

A distinct depositional trend is not observable in this layer-by-layer analysis, however, the igneous products associated with elements typical for felsic but also mafic minerals tend to be more abundant in the lower part of the outcrop. The middle part of the outcrop is dominated by Ca and F abundances while the upper part tend to contain again more felsic and mafic minerals.

4. Summary

During the measurements with the commercial handheld LIBS device in the field, it was not possible to bring the sample surface always in direct contact with the instrument due to a limited accessibility and naturally rough surfaces. Consequently, spectra had to be measured with varying distances between target and instrument. With the laboratory measurements made on a gypsum sample, we identified different trends for increasing distances between sample and handheld instrument of Ar and Ca emission lines coming from the atmosphere and the sample, respectively. The Ar emission lines,

which contain no geochemical information regarding the present field investigation, can not be used for data normalization. Nevertheless, the approach of rejecting spectra, which have a ratio between the integrated intensities above and below 650 nm larger than one, was shown to be a useful indicator for the quality of the spectra. We showed that the rejection threshold should be chosen according to the spectra depending on their typical emission lines. We found that LIBS data obtained with a distance of 40 mm or more between sample and device are of reduced quality and not useful for further analysis.

For this study, a dedicated pre-processing of the data was necessary. First approaches have shown that the influence of Ar emission lines coming from the atmosphere on the PCA is strong and covers therefore information of elemental variations. In order to avoid this, we masked all identified Ar emission lines in the spectra. Subsequently, each spectrum was normalized by its total emission intensity, mean centered, and its standard deviation was scaled to unity.

For the data exploration with PCA, score and loading plots up to PC 6 were discussed. Clustering or trends related to the color of the layers were not observed. However, for some individual layers similar trends for spectra of the same layer could be seen. Each PC revealed correlations with several combinations of elemental emission lines which allow therefore to do semi-quantitative estimates of elemental abundances for each spectrum, at least in relation to the other spectra. However, the loadings also show specific correlations with emission lines that are influenced by varying line shapes or line positions. From these correlations, deriving quantitative estimates is challenging as it is complicated to relate them to elemental abundances.

Moreover, effects from a varying angle between instrument and sample (line shifts) or self absorption are most likely responsible for these findings.

The layer-by-layer analysis of fitted emission lines revealed correlations mainly between elements typical for felsic and mafic minerals in contrast to an anti-correlation with Ca and F. This is in agreement with the expected igneous minerals at the measurement site which are rich in alkalis. However, as in the PCA, no clear relation of emission line intensities with the assigned layer color was identified, except that Fe seems to be more abundant in most red layers. Regarding minor and trace elements, several correlations could be identified.

From the present study, it can be concluded that LIBS indeed is a powerful elemental analysis technique even with the discussed challenges in field applications. However, if possible, experimental conditions should be kept as constant as possible between different measurements. The handheld LIBS instrument used in this work has a high ease of use but is also limited in its versatility because of the flat surface which has to be ideally put in full contact with the sample surface. All in all, compositional variations of the ash layers could be observed which was the objective of this study. The PCA as well as the fitted emission lines served as useful tools for the data exploration of the ash layers. The applied data pre-processing including the masking of Ar emission lines lead to the best outcomes regarding the traceability of elemental variations. In addition to the analysis, a better understanding of the performance and limitations of the LIBS device was obtained which can help to improve future field investigations using a handheld LIBS instrument but also give input into instrument designs for robotic or human in-situ explo-

ration.

In general, based on this study, we recommend to do more than three measurements at different positions on geological features which are suspected to have a similar or even same elemental composition. 14 % of our measurements had to be rejected due to insufficient data quality which left not enough data to derive statistically meaningful geochemical differences between the layers. With more measurements in one layer, better estimates for the homogeneity of the layers and the reproducibility of the LIBS measurements could have been possible. Another approach to improve the performance of the instrument could be a change in the measurement mode: Instead of integrating spectra of multiple induced plasmas, shot-to-shot measurements could be done in order to obtain data of the sample with increasing depth and to better understand underlying processes that influence the final LIBS spectrum. This procedure could also provide a measure of the homogeneity of sample surfaces. Regarding the instrument, we want to emphasize the importance to keep the sampling distance as small as possible and the angle constant to maximize the performance and quality of the data when measuring geological samples in the field. The sensitivity to the geometric positioning arises from the configuration of this specific instrument and a similar device for astronauts or hardware for an exploration rover should be designed in a way that is more robust to these kinds of effects.

5. Conclusions and outlook

In the present study, LIBS data from in-field measurements of volcanic ash layers using a handheld LIBS instrument were analyzed to evaluate the

easy of use of such LIBs devices for terrestrial and planetary geochemical exploration. Additionally, measurements in the laboratory with the same instrument were conducted in order to investigate the effect of varying distances between the sample and the device. An outcrop of volcanic ash on the Eolian island Vulcano (Italy), which provides excellent planetary analog sites, was measured within the framework of a Summer School held on the island Vulcano. In this study, we focused on the performance of a handheld LIBS device on geologically challenging and representative sample matrices and designed and investigated various data analysis strategies. We found that differences between the ash layers can be observed in the LIBS data. Correlations of elemental emission intensities confirmed the shoshonitc-alkaline character of the ashes. However, also challenges in field applications with the handheld LIBS device were identified which concern mainly the varying sample-instrument distance. Therefore, we give recommendations for future field investigations using LIBS handheld instrumentation.

As mentioned in the beginning, samples were not only measured by LIBS but also with VIS/NIR reflectance and Raman spectroscopy. In further studies, the combination of the data from these different spectroscopic techniques is planned which could further improve sample identification as they provide different types of data most likely enabling a more complete geological interpretation. Furthermore, dedicated calibration models for the handheld instrument in the particular conditions of field missions will be developed in order to provide quantitative results from future explorations.

Acknowledgements

The Summer School held on Vulcano is an extension and continuation of the successful previous four Summer Schools which were supported by the Helmholtz Alliance Robotic Exploration of Extreme Environments (ROBEX) and now generously supported by the EU Europlanet program. G.O. and F.S. acknowledge funding by the Deutsche Forschungsgemeinschaft (DFG, German Research Foundation) – Project-ID 263649064 – TRR 170. This is TRR 170 Publication No. XX..

References

[1] David W. Hahn and Nicoló Omenetto. Laser-induced breakdown spectroscopy (LIBS), part II: Review of instrumental and methodological approaches to material analysis and applications to different fields. *Applied Spectroscopy*, 66(4):347–419, 2012.

[2] Reinhard Noll, Holger Bette, Adriane Brysch, Marc Kraushaar, Ingo Mönch, Laszlo Peter, and Volker Sturm. Laser-induced breakdown spectrometry - Applications for production control and quality assurance in the steel industry. *Spectrochimica Acta - Part B Atomic Spectroscopy*, 56(6):637–649, 2001.

[3] Patrick Mauchien, Agnés Pailloux, and Thomas Vercouter. Applications of laser spectroscopy in nuclear research and industry. In *Laser Spectroscopy for Sensing: Fundamentals, Techniques and Applications*, pages 522–543. Woodhead Publishing, 2014.

667 [4] Maria Markiewicz-Keszycka, Xavier Cama-Moncunill, Maria P. Casado-
668 Gavalda, Yash Dixit, Raquel Cama-Moncunill, Patrick J. Cullen, and
669 Carl Sullivan. Laser-induced breakdown spectroscopy (LIBS) for food
670 analysis: A review. *Trends in Food Science and Technology*, 65:80–93,
671 2017.

672 [5] Asia Botto, Beatrice Campanella, Stefano Legnaioli, Marco Lezzerini,
673 Giulia Lorenzetti, Stefano Pagnotta, Francesco Poggialini, and Vincenzo
674 Palleschi. Applications of laser-induced breakdown spectroscopy in cul-
675 tural heritage and archaeology: A critical review. *Journal of Analytical*
676 *Atomic Spectrometry*, 34(1):81–103, 2019.

677 [6] Cécile Fabre. Advances in Laser-Induced Breakdown Spectroscopy anal-
678 ysis for geology: A critical review. *Spectrochimica Acta - Part B Atomic*
679 *Spectroscopy*, 166(February):105799, 2020.

680 [7] Russell S. Harmon, Richard E. Russo, and Richard R. Hark. Appli-
681 cations of laser-induced breakdown spectroscopy for geochemical and
682 environmental analysis: A comprehensive review. *Spectrochimica Acta*
683 *- Part B Atomic Spectroscopy*, 87:11–26, 2013.

684 [8] Giorgio S. Senesi. Laser-Induced Breakdown Spectroscopy (LIBS) ap-
685 plied to terrestrial and extraterrestrial analogue geomaterials with em-
686 phasis to minerals and rocks. *Earth-Science Reviews*, 139:231–267, 2014.

687 [9] S Maurice, R C Wiens, M Saccoccio, B Barraclough, O Gasnault,
688 O Forni, N Mangold, D Baratoux, S Bender, G Berger, J Bernardin,
689 M Berthé, N Bridges, D Blaney, M Bouyé, P Caïs, B Clark, S Clegg,

690 A Cousin, D Cremers, A Cros, L Deflores, C Derycke, B Dingler, G Dro-
691 mart, B Dubois, M Dupieux, E Durand, L D'Uston, C Fabre, B Faure,
692 A Gaboriaud, T Gharsa, K Herkenhoff, E Kan, L Kirkland, D Kouach,
693 J L Lacour, Y Langevin, J Lasue, S Le Mouélic, M Lescure, E Lewin,
694 D Limonadi, G Manhès, P Mauchien, C McKay, P Y Meslin, Y Michel,
695 E Miller, H E Newsom, G Orttner, A Paillet, L Parès, Y Parot, R Pérez,
696 P Pinet, F Poitrasson, B Quertier, B Sallé, C Sotin, V Sautter, H Séran,
697 J J Simmonds, J B Sirven, R Stiglich, N Striebig, J J Thocaven, M J
698 Toplis, and D Vaniman. The ChemCam instrument suite on the Mars
699 Science Laboratory (MSL) rover: Science objectives and mast unit de-
700 scription. *Space Science Reviews*, 170(1-4):95–166, 2012.

701 [10] Roger C. Wiens, Sylvestre Maurice, Bruce Barraclough, Muriel Saccoc-
702 cio, Walter C. Barkley, James F. Bell, Steve Bender, John Bernardin, Di-
703 ana Blaney, Jennifer Blank, Marc Bouyé, Nathan Bridges, Nathan Bult-
704 man, Phillippe Caïs, Robert C. Clanton, Benton Clark, Samuel Clegg,
705 Agnes Cousin, David Cremers, Alain Cros, Lauren Deflores, Dorothea
706 Delapp, Robert Dingler, Claude D'Uston, M. Darby Dyar, Tom Elliott,
707 Don Enemark, Cecile Fabre, Mike Flores, Olivier Forni, Olivier Gas-
708 nault, Thomas Hale, Charles Hays, Ken Herkenhoff, Ed Kan, Laurel
709 Kirkland, Driss Kouach, David Landis, Yves Langevin, Nina Lanza,
710 Frank Larocca, Jeremie Lasue, Joseph Latino, Daniel Limonadi, Chris
711 Lindensmith, Cynthia Little, Nicolas Mangold, Gerard Manhes, Patrick
712 Mauchien, Christopher McKay, Ed Miller, Joe Mooney, Richard V.
713 Morris, Leland Morrison, Tony Nelson, Horton Newsom, Ann Ollila,
714 Melanie Ott, Laurent Pares, René Perez, Franck Poitrasson, Cheryl

715 Provost, Joseph W. Reiter, Tom Roberts, Frank Romero, Violaine Sautter, Steven Salazar, John J. Simmonds, Ralph Stiglich, Steven Storms, Nicolas Striebig, Jean Jacques Thocaven, Tanner Trujillo, Mike Ulibarri, David Vaniman, Noah Warner, Rob Waterbury, Robert Whitaker, James Witt, and Belinda Wong-Swanson. The ChemCam instrument suite on the Mars Science Laboratory (MSL) rover: Body unit and combined system tests. *Space Science Reviews*, 170(1-4):167–227, 2012.

[11] S. Maurice, S. M. Clegg, R. C. Wiens, O. Gasnault, W. Rapin, O. Forni, A. Cousin, V. Sautter, N. Mangold, L. Le Deit, M. Nachon, R. B. Anderson, N. L. Lanza, C. Fabre, V. Payré, J. Lasue, P. Y. Meslin, R. J. Léveillé, B. L. Barraclough, P. Beck, S. C. Bender, G. Berger, J. C. Bridges, N. T. Bridges, G. Dromart, M. D. Dyar, R. Francis, J. Frydenvang, B. Gondet, B. L. Ehlmann, K. E. Herkenhoff, J. R. Johnson, Y. Langevin, M. B. Madsen, N. Melikechi, J. L. Lacour, S. Le Mouélic, E. Lewin, H. E. Newsom, A. M. Ollila, P. Pinet, S. Schröder, J. B. Sirven, R. L. Tokar, M. J. Toplis, C. D'Uston, D. T. Vaniman, and A. R. Vasavada. ChemCam activities and discoveries during the nominal mission of the Mars Science Laboratory in Gale crater, Mars. *Journal of Analytical Atomic Spectrometry*, 31(4):863–889, 2016.

[12] Andrew K. Knight, Nancy L. Scherbarth, David A. Cremers, and Monty J. Ferris. Characterization of laser-induced breakdown spectroscopy (LIBS) for application to space exploration. *Applied Spectroscopy*, 54(3):331–340, 2000.

[13] Roger C. Wiens, Sylvestre Maurice, and Fernando Rull Perez. The

SuperCam Remote Sensing Instrument Suite for the Mars 2020 Rover: A Preview. *Spectroscopy*, 32(5):50–55, 2017.

[14] A.S. Laxmiprasad, V.L.N. Sridhar Raja, Surya Menon, Adwaita Goswami, M.V.H. Rao, and K.A. Lohar. An in situ laser induced breakdown spectroscope (libs) for chandrayaan-2 rover: Ablation kinetics and emissivity estimations. *Advances in Space Research*, 52(2):332 – 341, 2013. Lunar Exploration - II.

[15] X. Ren, T. N. Cai, D. W. Liu, J. J. Liu, H. B. Zhang, Q. Fu, Z. B. Zhang, and W. M. Xu. Preliminary Scientific Exploration Programs for Mars Surface Composition Detection Package of China's First Mars Exploration. In *12th European Planetary Science Congress*, page Abstract #759, Berlin, Germany, 2018.

[16] J. Lasue, R. C. Wiens, S. M. Clegg, D. T. Vaniman, K. H. Joy, S. Humphries, A. Mezzacappa, N. Melikechi, R. E. McInroy, and S. Bender. Remote laser-induced breakdown spectroscopy (LIBS) for lunar exploration. *Journal of Geophysical Research E: Planets*, 117(1), 2012.

[17] S. G. Pavlov, S. Schröder, I. Rauschenbach, E. K. Jessberger, and H. W. Hübers. Low-energy laser induced breakdown spectroscopy for in-situ space missions to solar system bodies without atmospheres. *Planetary and Space Science*, 2012.

[18] S. M. Clegg, M. D. Dyar, R. T. Newell, C. G. Peterson, D. S. DeCroix, B. S. Okhuysen, S. K. Sharma, S. Maurice, R. C. Wiens, and L. S. Glaze. Venus elemental and mineralogical camera (vemcam). In *49th*

762 *Lunar and Planetary Science Conference*, page Abstract #2676, The
763 Woodlands, USA, 2018. Lunar and Planetary Institute.

764 [19] David A Cremers and Leon J Radziemski. *Handbook of laser induced*
765 *breakdown spectroscopy*. Wiley, Chichester, 2. ed. edition, 2013.

766 [20] W. D. Hahn and N. Omenetto. Laser-Induced Breakdown Spectroscopy
767 (LIBS), Part I: Review of Basic Diagnostics and Plasma-Particle Inter-
768 actions: Still-Challenging Issues Within the Analytical Plasma Commu-
769 nity. *Appl. Spectrosc.*, 64:335A–366A, 2010.

770 [21] J. El Haddad, L. Canioni, and B. Bousquet. Good practices in LIBS
771 analysis: Review and advices. *Spectrochimica Acta Part B: Atomic Spec-*
772 *troscopy*, 101:171–182, nov 2014.

773 [22] Sarah C. Jantzi, Vincent Motto-Ros, Florian Trichard, Yuri Markushin,
774 Noureddine Melikechi, and Alessandro De Giacomo. Sample treatment
775 and preparation for laser-induced breakdown spectroscopy. *Spectrochim-*
776 *ica Acta Part B: Atomic Spectroscopy*, 115:52–63, jan 2016.

777 [23] R Tessadri. Introduction to the mineralogical sciences. pt 3: An-
778 alytical techniques for elemental analysis of minerals. In *UN-*
779 *ESCO—Encyclopedia of Life Support Systems EOLSS*. on-line, publi-
780 cation, www.eolss.net, 2003.

781 [24] John L Campbell, Glynis M Perrett, Ralf Gellert, Stefan M An-
782 drushenko, Nicholas I Boyd, John A Maxwell, Penelope L King, and
783 Céleste DM Schofield. Calibration of the mars science laboratory alpha

particle x-ray spectrometer. *Space Science Reviews*, 170(1-4):319–340, 2012.

[25] Elisabetta Tognoni and Gabriele Cristoforetti. Signal and noise in Laser Induced Breakdown Spectroscopy: An introductory review. *Optics and Laser Technology*, 79(May):164–172, 2016.

[26] J.-B. Sirven, B. Bousquet, L. Canioni, and L. Sarger. Laser-Induced Breakdown Spectroscopy of Composite Samples: Comparison of Advanced Chemometrics Methods. *Analytical Chemistry*, 78(5):1462–1469, 2006.

[27] G De Astis, F Lucchi, P Dellino, L La Volpe, C A Tranne, M L Frezzotti, and A Peccerillo. Chapter 11 Geology, volcanic history and petrology of Vulcano (central Aeolian archipelago). *Geological Society, London, Memoirs*, 37(1):281 LP – 349, 2013.

[28] Stefano Rossi, Maurizio Petrelli, Daniele Morgavi, Francesco P. Vetere, Renat R. Almeev, Rebecca L. Astbury, and Diego Perugini. Role of magma mixing in the pre-eruptive dynamics of the Aeolian Islands volcanoes (Southern Tyrrhenian Sea, Italy). *Lithos*, 324-325:165–179, 2019.

[29] K. Stephan, S. Schröder, M. Baqué, K. Rammelkamp, J. Haber, I. Varatharajan, G. Ortenzi, A. Pisello, R. Pasek, F. Sohl, R. Jaumann, L. Thomson, and V. Unnithan. Multi-spectral investigation of volcanic deposits and their alteration processes on Vulcano/ Italy. In *13th*

European Planetary Science Congress, page Abstract #2062, Geneva, Switzerland, 2019.

[30] K. Stephan, S. Schröder, M. Baqué, K. Rammelkamp, J. Haber, I. Varatharajan, G. Ortenzi, A. Pisello, R. Pasek, F. Sohl, R. Jaumann, L. Thomson, and V. Unnithan. Multi-spectral investigation of planetary analog material in extreme environments - alteration products of volcanic deposits of Vulcano/Italy. In *51th Lunar and Planetary Science Conference*, page Abstract #2411, The Woodlands, USA, 2020.

[31] Lionel Wilson. Volcanism in the solar system. *Nature Geoscience*, 2(6):389, 2009.

[32] Brendan Connors, Andrew Somers, and David Day. Application of Handheld Laser-Induced Breakdown Spectroscopy (LIBS) to Geochemical Analysis. *Applied Spectroscopy*, 70(5):810–815, 2016.

[33] Russell S. Harmon, Richard R. Hark, Chandra S. Throckmorton, Eugene C. Rankey, Michael A. Wise, Andrew M. Somers, and Leslie M. Collins. Geochemical Fingerprinting by Handheld Laser-Induced Breakdown Spectroscopy. *Geostandards and Geoanalytical Research*, 41(4):563–584, 2017.

[34] Russell S. Harmon, Chandra S. Throckmorton, Richard R. Hark, Jennifer L. Gottfried, Gerhard Wörner, Karen Harpp, and Leslie Collins. Discriminating volcanic centers with handheld laser-induced breakdown spectroscopy (LIBS). *Journal of Archaeological Science*, 98(July):112–127, 2018.

[35] Y. Foucaud, C. Fabre, B. Demeusy, I. V. Filippova, and L. O. Filippov. Optimisation of fast quantification of fluorine content using handheld laser induced breakdown spectroscopy. *Spectrochimica Acta - Part B Atomic Spectroscopy*, 158:105628, 2019.

[36] Cai R. Ytsma, Christine A. Knudson, M. Darby Dyar, Amy C. McAdam, Danielle D. Michaud, and Lindsey M. Rollosson. Accuracies and detection limits of major, minor, and trace element quantification in rocks by portable laser-induced breakdown spectroscopy. *Spectrochimica Acta Part B: Atomic Spectroscopy*, 171(July):105946, sep 2020.

[37] M. H. Yant, K. W. Lewis, A. H. Parker, S. M. Hörst, A. C. McAdam, and C. A. Knudson. Project espresso: Exploration roles of handheld libs at the potrillo volcanic field. In *50th Lunar and Planetary Science Conference*, page Abstract #2645, Houston, 2019. Lunar and Planetary Institute.

[38] Giorgio S. Senesi, Russell S. Harmon, and Richard R. Hark. Field-portable and handheld laser-induced breakdown spectroscopy: Historical review, current status and future prospects. *Spectrochimica Acta Part B: Atomic Spectroscopy*, 175(October 2020):106013, jan 2021.

[39] Bernard Foing. Overview of moon village global activities & lunar explorers tribute. In *EGU General Assembly Conference Abstracts*, volume 20, page 18534, 2018.

[40] Yasuo Iida. Effects of atmosphere on laser vaporization and excitation

processes of solid samples. *Spectrochimica Acta Part B: Atomic Spectroscopy*, 45(12):1353–1367, 1990.

[41] R.J. Lasheras, C. Bello-Gálvez, and J.M. Anzano. Quantitative analysis of oxide materials by laser-induced breakdown spectroscopy with argon as an internal standard. *Spectrochimica Acta Part B: Atomic Spectroscopy*, 82:65–70, 2013.

[42] A. De Giacomo, M. Dell'Aglio, R. Gaudiuso, S. Amoruso, and O. De Pascale. Effects of the background environment on formation, evolution and emission spectra of laser-induced plasmas. *Spectrochimica Acta Part B: Atomic Spectroscopy*, 78:1–19, 2012.

[43] Jörg Hermann, Christoph Gerhard, Emanuel Axente, and Christophe Dutouquet. Comparative investigation of laser ablation plumes in air and argon by analysis of spectral line shapes: Insights on calibration-free laser-induced breakdown spectroscopy. *Spectrochimica Acta Part B: Atomic Spectroscopy*, 100:189–196, 2014.

[44] S. Schröder, K. Rammelkamp, D.S. Vogt, O. Gasnault, and H.-W. Hübers. Contribution of a martian atmosphere to laser-induced breakdown spectroscopy (LIBS) data and testing its emission characteristics for normalization applications. *Icarus*, 325(December 2018):1–15, 2019.

[45] A. Kramida, Yu. Ralchenko, J. Reader, and and NIST ASD Team. NIST Atomic Spectra Database (ver. 5.7.1), [Online]. Available: `https://physics.nist.gov/asd` [2020, March 12]. National Institute of Standards and Technology, Gaithersburg, MD., 2019.

[46] G. De Astis, L. La Volpe, A. Peccerillo, and L. Civetta. Volcanological and petrological evolution of Vulcano island (Aeolian Arc, southern Tyrrhenian Sea). *Journal of Geophysical Research: Solid Earth*, 102(B4):8021–8050, 1997.

[47] Raffaella Fusillo, Federico Di Traglia, Anna Gioncada, Marco Pistolesi, Paul J. Wallace, and Mauro Rosi. Deciphering post-caldera volcanism: insight into the Vulcanello (Island of Vulcano, Southern Italy) eruptive activity based on geological and petrological constraints. *Bulletin of Volcanology*, 77(9), 2015.

[48] M. Gaft, L. Nagli, N. Eliezer, Y. Groisman, and O. Forni. Elemental analysis of halogens using molecular emission by laser-induced breakdown spectroscopy in air. *Spectrochimica Acta - Part B Atomic Spectroscopy*, 98:39–47, 2014.

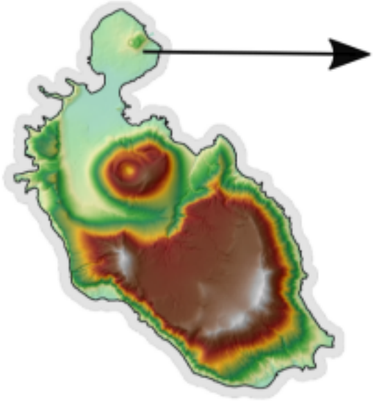
[49] Olivier Forni, Michael Gaft, Michael J. Toplis, Samuel M. Clegg, Sylvestre Maurice, Roger C. Wiens, Nicolas Mangold, Olivier Gasnault, Violaine Sautter, Stéphane Le Mouélic, Pierre Yves Meslin, Marion Nachon, Rhonda E. McInroy, Ann M. Ollila, Agnès Cousin, John C. Bridges, Nina L. Lanza, and Melinda D. Dyar. First detection of fluorine on Mars: Implications for Gale Crater's geochemistry. *Geophysical Research Letters*, 42(4):1020–1028, 2015.

[50] D.S. Vogt, S. Schröder, K. Rammelkamp, P.B. Hansen, S. Kubitza, and H.-W. Hübers. CaCl and CaF emission in LIBS under simulated Martian conditions. *Icarus*, 335:113393, 2020.

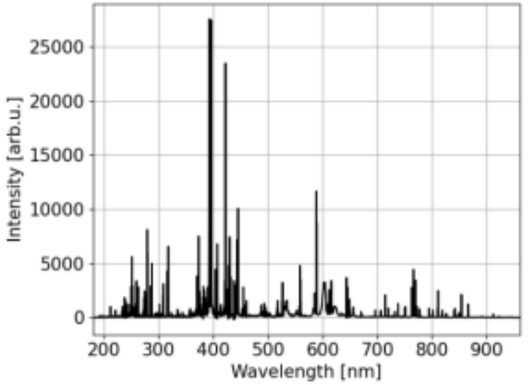
[51] Igor B. Gornushkin, Leslie A. King, Ben W. Smith, Nicoló Omenetto, and James D. Winefordner. Line broadening mechanisms in the low pressure laser-induced plasma. *Spectrochimica acta, Part B: Atomic spectroscopy*, 54(8):1207–1217, 1999.

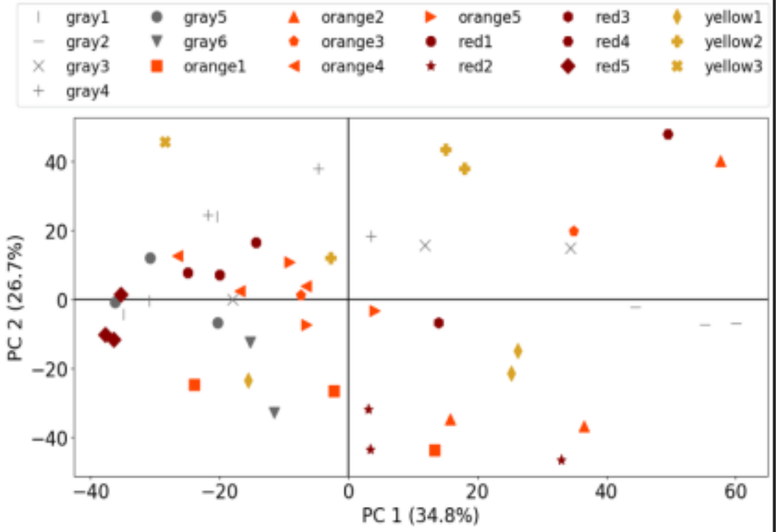
[52] Koo Hendrik Kurniawan, May On Tjia, and Kiichiro Kagawa. Review of Laser-Induced Plasma, Its Mechanism, and Application to Quantitative Analysis of Hydrogen and Deuterium. *Applied Spectroscopy Reviews*, 49(5):323–434, 2014.

[53] D. S. Vogt, K. Rammelkamp, S. Schröder, and H. W. Hübers. Molecular emission in laser-induced breakdown spectroscopy: An investigation of its suitability for chlorine quantification on Mars. *Icarus*, 302:470–482, 2018.






Intensity [arb.u.]
25000
20000
15000
10000
5000
0
200
300
400
500
600
700
800
900
Wavelength [nm]


gray1
gray2
gray3
gray4
gray5
gray6
orange1
orange2
orange3
orange4
orange5
red1
red2
red3
red4
red5
yellow1
yellow2
yellow3
PC 2 (26.7%)
PC 1 (34.8%)